Monthly Notices
of the
ROYAL ASTRONOMICAL SOCIETY

MNRAS **495,** 1927–1933 (2020)
Advance Access publication 2020 May 14

doi:10.1093/mnras/staa1287

ExoMol line lists – XXXVIII. High-temperature molecular line list of silicon dioxide (SiO_2)

A. Owens,[1] E. K. Conway ,[1,2] J. Tennyson [1]★ and S. N. Yurchenko[1]

[1]*Department of Physics and Astronomy, University College London, Gower Street, WC1E 6BT London, UK*
[2]*Atomic and Molecular Physics Division, Center for Astrophysics, Harvard and Smithsonian, Cambridge, MA 02138, USA*

Accepted 2020 May 5. Received 2020 May 5; in original form 2020 February 24

ABSTRACT

Silicon dioxide (SiO_2) is expected to occur in the atmospheres of hot rocky super-Earth exoplanets but a lack of spectroscopic data is hampering its possible detection. Here, we present the first, comprehensive molecular line list for SiO_2. The line list, named OYT3, covers the wavenumber range 0 – 6000 cm^{-1} (wavelengths $\lambda > 1.67$ μm) and is suitable for temperatures up to $T = 3000$ K. Almost 33 billion transitions involving 5.69 million rotation–vibration states with rotational excitation up to $J = 255$ have been computed using robust first-principles methodologies. The OYT3 line list is available from the ExoMol data base at www.exomol.com.

Key words: molecular data – opacity – planets and satellites: atmospheres – stars: atmospheres – ISM: molecules.

1 INTRODUCTION

In the gas phase, silicon dioxide ($^{28}Si^{16}O_2$) is a linear triatomic molecule, analogous to CO_2. SiO_2 is expected to be present in the atmospheres of hot rocky super-Earth exoplanets (Tennyson & Yurchenko 2017a). These tidally locked exoplanets are in close proximity to their host star with their dayside exposed to temperatures reaching 4000 K. At such high temperatures the material on the surface of the planet vaporizes to produce an atmosphere strongly dependent on initial planetary composition (Schaefer & Fegley 2009; Miguel et al. 2011), e.g. composed of SiO_2-rich silicates like the Earth's continental crust (Schaefer, Lodders & Fegley 2012). Furthermore, the likely presence of water vapour creates a steam atmosphere, and since all major rock-forming elements (Si, Mg, Ca, etc.) dissolve in steam to some extent, one can expect to encounter simple molecules composed of rock-forming elements with oxygen and hydrogen (Fegley et al. 2016).

Investigating the spectroscopy of hot rocky super-Earths requires accurate molecular opacities on systems such as SiO_2. There is, however, very limited information on some of these molecules, partly because they form in the gas phase at very high temperatures making their spectra challenging to measure in the laboratory. Instead, theory offers a more viable route for generating the molecular line lists of these systems through systematic approaches based on first-principles methodologies (Tennyson 2016; Tennyson & Yurchenko 2017b). These computational procedures have been successfully adopted by the ExoMol data base (Tennyson & Yurchenko 2012; Tennyson et al. 2016), which provides comprehensive line lists suitable for modelling exoplanet atmospheres at elevated temperatures. Already a large number of important diatomic and polyatomic species have been treated within the ExoMol framework (Tennyson & Yurchenko 2018), and efforts are now being focused on molecules relevant to hot rocky super-Earth atmospheres. This brings about its own unique set of challenges, notably the completeness of the line list at very high temperatures and the lack of experimental data to refine the theoretical spectroscopic model.

Regarding SiO_2, only a few studies have investigated its infrared spectrum with measurements of the ν_2 bending mode (Andrews & McCluskey 1992) and ν_3 stretching mode (Schnöckel 1978, 1980). However, since these studies were performed in solid argon matrices the measured wavenumbers can be shifted by tens of wavenumbers (Jacox 1994) making it difficult to assess the usefulness of the determined values for gas phase studies. Similarly, only a small number of theoretical studies have considered silicon dioxide (Kaufman, Muenter & Klemperer 1967; Pacansky & Hermann 1978; Wang et al. 1996; Brinkmann, Tschumper & Schaefer III 1999; Kostko, Ahmed & Metz 2009; Hao, Xie & Schaefer 2014), but none of these are particularly relevant to the work presented here, namely the high-accuracy calculation of its rotation–vibration spectrum.

In this work, we present the first, comprehensive rotation–vibration line list of gas-phase SiO_2. The new line list has been computed using robust first-principles methodologies (Tennyson 2016) within the ExoMol computational framework (Tennyson & Yurchenko 2017b) and adds to the other available silicon-bearing molecules in the ExoMol data base: SiH_4 (Owens et al. 2017), SiH (Gorman, Yurchenko & Tennyson 2019), SiO (Barton, Yurchenko & Tennyson 2013), SiS (Upadhyay et al. 2018), and SiH_2 (Clark et al. 2020).

★ E-mail: j.tennyson@ucl.ac.uk

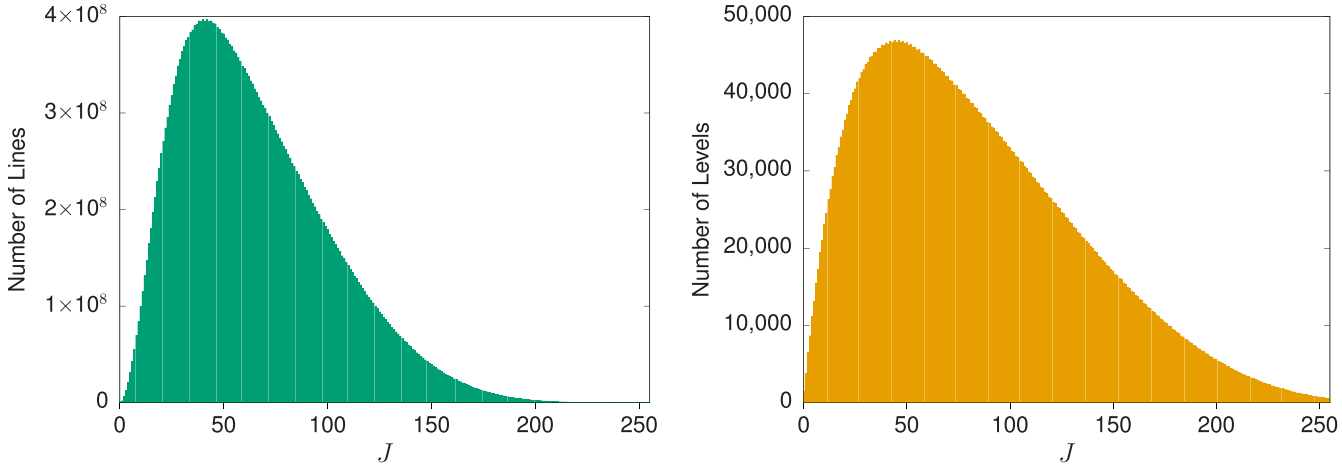

Figure 1. The total number of lines (left-hand panel) and energy levels (right-hand panel) for each value of the rotational quantum number J in the OYT3 line list. For the number of lines, a single J value counts transitions between $J \leftrightarrow J-1$ and $J \leftrightarrow J$.

2 METHODS

The computational approach used to produce the SiO_2 line list is described in detail in the supplementary material and only a brief summary is provided here. Initially, high-level ab initio methods were used to compute the potential energy surface (PES) and dipole moment surface (DMS) of the electronic ground state of SiO_2. The PES was generated using explicitly correlated coupled cluster (CCSD(T)-F12b) calculations with extrapolation to the complete basis set limit, and included several additive energy corrections to account for small effects like scalar relativity. This approach is capable of producing accurate PESs for closed-shell molecules that can reproduce fundamental term values to within $\pm 1\,\mathrm{cm}^{-1}$ on average (e.g. see Owens et al. 2018 and references within). Due to the lack of reliable experimental data for this molecule, the PES was not empirically refined. The DMS was computed using CCSD(T)-F12b with a large augmented correlation consistent basis set. It is now well established that transition intensities computed using ab initio DMSs are comparable to, and occasionally more reliable, than experiment (Tennyson 2014; Yurchenko 2014). Both surfaces were computed on the same grid of 15 365 nuclear geometries and then fitted with suitable analytic representations for use in the next stage of the calculation process. The potential energy and dipole moment surfaces are provided as supplementary material along with Fortran routines to construct them.

Line list calculations employed the variational nuclear motion program TROVE (Yurchenko, Thiel & Jensen 2007), which was extended to treat linear triatomic molecules in this work. Benchmarking was performed against the triatomic nuclear motion code DVR3D (Tennyson et al. 2004) to ensure the validity of the TROVE implementation. The ability to utilize two nuclear motion codes based on different methodologies proved highly beneficial and meant the theoretical spectroscopic model of SiO_2 could be checked for consistency. This was particularly important given the lack of experimental data to compare against. A large symmetry-adapted basis set was used in the rovibrational calculations with convergence testing performed at different J values.

The line list was computed with a lower state energy threshold of $hc \cdot 15\,000\,\mathrm{cm}^{-1}$ (h is the Planck constant and c is the speed of light) and considered transitions up to $J = 255$ in the $0-6000\,\mathrm{cm}^{-1}$ range. The energy levels and wavefunctions of SiO_2 can be classified under the $\boldsymbol{C}_{2v}$(M) molecular symmetry group (Bunker & Jensen 1998). The nuclear spin statistical weights are $g_{ns} = \{1, 1, 0, 0\}$ for states of symmetry $\{A_1, A_2, B_1, B_2\}$, respectively. Thus, B_1 and B_2 states need not be computed and transitions follow the symmetry selection rules $A_1 \leftrightarrow A_2$; and the standard rotational selection rules, $J' - J'' = 0, \pm 1, J' + J'' \neq 0$; where $'$ and $''$ denote the upper and lower state, respectively. These representations are correlated to the $\boldsymbol{D}_{\infty h}$(M) irreducible representations, commonly used for linear molecules, as $A_1 \leftrightarrow \Sigma_g^+$ and $A_2 \leftrightarrow \Sigma_u^-$. Another standard spectroscopic descriptor is the Kronig parity e/f (Brown et al. 1975), related to the total parity $+1$ (A_1) and -1 (A_2) as follows: the parity of the e state is $(-1)^J$ while the parity of the f state is $(-1)^{J+1}$.

The vibrational quantum numbers used by TROVE (see supplementary material) were correlated to the following standard spectroscopic quantum numbers used for linear-type triatomic molecules: v_1, v_2^{lin}, $L = |l|$, v_3, where v_1 and v_3 are the symmetric and asymmetric stretching quantum numbers, respectively, v_2 is the bending vibrational quantum number used for linear molecules and l is the corresponding vibrational quantum number. The two bending quantum numbers v_2^{lin} and l are connected to the 'non-linear' bending quantum number v_2 by $v_2^{\mathrm{lin}} = 2v_2 + l$ with $L = v_2^{\mathrm{lin}}, v_2^{\mathrm{lin}} - 2, \ldots 0(1)$.

The symmetries of the vibrational and rotational contributions span the A_1, A_2, B_1, and B_2 irreducible representations (irreps) in $\boldsymbol{C}_{2v}$(M) and $\Sigma_{g/u}^{+/-}$ ($L = 0$), $\Pi_{g/u}$ ($L = 1$), $\Delta_{g/u}$ ($L = 2$) etc. in $\boldsymbol{D}_{\infty h}$. Odd values of the quantum number v_3 indicates vibrational states of B_2 symmetry. The rotational quantum number k_a is constrained to the vibrational angular momentum by $k_a = l$.

A total of 32 951 275 437 transitions involving 5 688 942 energy levels up to $J = 255$ were computed for the OYT3 line list. The distribution of lines and levels as a function of J is illustrated in Fig. 1. The largest number of transitions in the OYT3 line list occurs between $J = 39 \leftrightarrow 40$, while the number of states peaks at $J = 46$ before smoothly decreasing, a result of the upper state energy threshold of $hc \cdot 21\,000\,\mathrm{cm}^{-1}$.

3 RESULTS

3.1 Partition function of silicon dioxide

The temperature-dependent partition function $Q(T)$ is expressed as,

$$Q(T) = \sum_i g_i \exp\left(\frac{-E_i}{kT}\right), \quad (1)$$

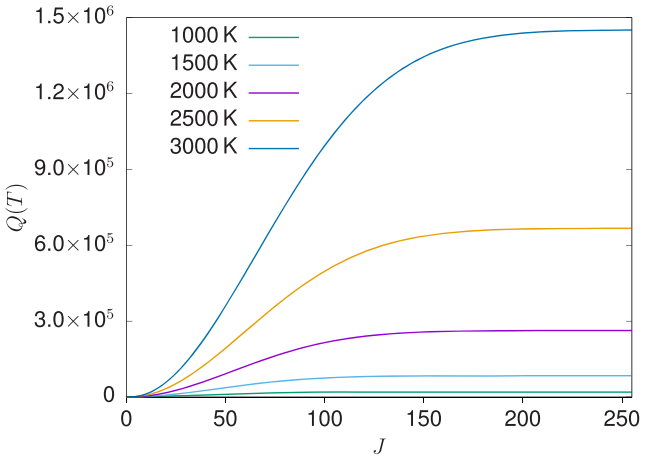

Figure 2. Convergence of the partition function $Q(T)$ of SiO_2 with respect to the rotational quantum number J at different temperatures.

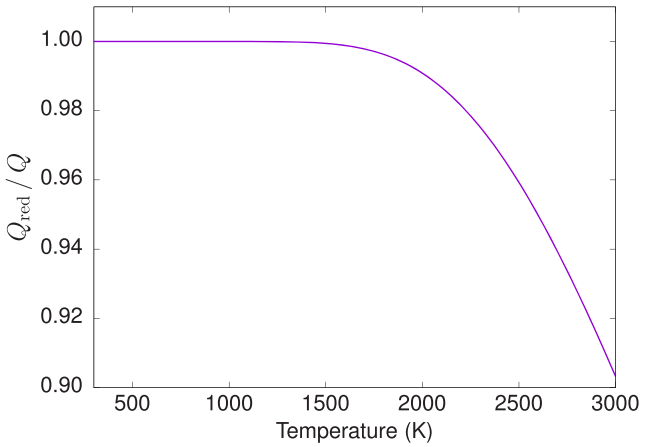

Figure 3. The ratio $Q_{\rm red}/Q$ as a function of temperature T; this provides a measure of the completeness of the OYT3 line list.

where $g_i = g_{\rm ns}(2J_i + 1)$ is the degeneracy of a state i with energy E_i and rotational quantum number J_i. Values of the partition function of SiO_2 have been computed by summing over all calculated rovibrational energy levels on a 1 K grid in the 1–3000 K range (provided as supplementary material). In Fig. 2, the convergence of $Q(T)$ as a function of J for select temperatures is shown. At lower temperatures the partition function converges quickly but a substantial number of high J states must be considered to achieve convergence above 1500 K. At $J = 255$, the value of $Q(2000\,{\rm K})$ is converged to 0.0001 per cent, while the value of $Q(3000\,{\rm K})$ is converged to 0.0019 per cent.

The SiO_2 line list was computed with a lower state energy threshold of $hc \cdot 15\,000\,{\rm cm}^{-1}$. A measure of the completeness of the line list can be obtained by studying the reduced partition function $Q_{\rm red}(T)$, which only includes energy levels up to $hc \cdot 15\,000\,{\rm cm}^{-1}$ in the summation of equation (1). The ratio $Q_{\rm red}(T)/Q(T)$ has been plotted with respect to temperature in Fig. 3 and from this we see that above 1500 K the ratio starts to decrease from unity. At 3000 K, the ratio $Q_{\rm red}/Q = 0.90$ and this should be considered as a soft temperature limit for the OYT3 line list. Uses above this will result in a progressive loss of opacity but the missing opacity contribution can be estimated from $Q_{\rm red}/Q$ if needed (Neale, Miller & Tennyson 1996).

3.2 Line list format

The SiO_2 line list is provided in the ExoMol data format and further details with illustrative examples can be found in Tennyson et al. (2016). The `.states` file, see Table 1, contains all the computed rovibrational energy levels (in $\rm cm^{-1}$), each labelled with a unique state ID counting number, symmetry and quantum number labelling, and the contribution C_i from the largest eigencoefficient used to assign the rovibrational state. The `.trans` files have been split into $100\,{\rm cm}^{-1}$ frequency bins for user-handling purposes and contain all computed transitions with upper and lower state ID labels and Einstein A coefficients, see Table 2.

The assignment of the vibrational quantum numbers to each state is performed in TROVE by analysing the contribution from the primitive basis functions of the different modes, which are then converted to the linear-molecule, normal mode quantum numbers (see Table 1). The connection between the assignment and the primitive basis functions is not always straightforward due to the complicated contraction scheme used to build the final symmetrized rovibrational basis set (Yurchenko, Yachmenev & Ovsyannikov 2017). Thus, in instances where the eigen-coefficient $|C_i|$ is very small the assignment should be considered as indicative.

The computed energy levels in the OYT3 line list have been assigned uncertainties (in $\rm cm^{-1}$) in the following way: The three fundamental term values have been given an estimated uncertainty of $2\,{\rm cm}^{-1}$, which has then been propagated to all overtone and combination bands using the TROVE normal mode quantum numbers. For example, a state with $(n_1 = 5, n_2 = 2, n_3 = 1)$ has an estimated uncertainty of $16\,{\rm cm}^{-1}$. The initial uncertainty estimate of $2\,{\rm cm}^{-1}$ for the fundamentals is based on our previous experience using similar levels of ab initio theory to construct closed-shell molecule potential energy surfaces (Owens et al. 2015a,b, 2016, 2018; Owens & Yurchenko 2019). This uncertainty scheme is approximate and should not be relied on in instances where the eigen-coefficient $|C_i|$ is small. We have also opted to round the estimated uncertainties to integer values so that they can be easily differentiated from more robust uncertainties, e.g. derived from experiment. Note that the ground state $J > 0$ rovibrational term values, i.e. $(n_1 = 0, n_2 = 0, n_3 = 0)$ have been assigned uncertainties of $2\,{\rm cm}^{-1}$ throughout.

3.3 Simulated spectra of silicon dioxide

The temperature dependence of the OYT3 line list is illustrated in Fig. 4, where we have plotted integrated absorption cross-sections at a resolution of $1\,{\rm cm}^{-1}$ using a Gaussian profile with a half-width at half-maximum (HWHM) of $1\,{\rm cm}^{-1}$. Spectral simulations were performed with the EXOCROSS program (Yurchenko, Al-Refaie & Tennyson 2018). As expected, the SiO_2 spectrum becomes smoother and more featureless as the temperature increases. This is caused by the increased population of vibrationally excited states with temperature, leading to substantial broadening of the rotational band envelopes.

Stick spectra of the two strongest bands at a temperature of 1000 K are shown in Fig. 5, with the fundamental ν_2 bending mode (left-hand panel) and the stretching ν_3 band (right-hand panel) displayed. The position of these bands is in broad agreement with previous experimental studies (Schnöckel 1978, 1980; Andrews & McCluskey 1992) but given these infrared measurements were performed in solid argon matrices, which are known to shift the measured wavenumbers, we avoid a direct comparison.

The SiO_2 spectrum has a distinct strong feature at 4.5 μm. This region plays an important role in the atmospheric applications of

Table 1. Extract from the `.states` file of the SiO_2 OYT3 line list.

i	$\tilde{E}$	$g_{\rm tot}$	J	unc	$\Gamma_{\rm tot}$	e/f	v_1	$v_2^{\rm lin}$	L	v_3	C_i	n_1	n_2	n_3	$\Gamma_{\rm vib}$	K	$\Gamma_{\rm rot}$
1	0.000000	1	0	0.000000	A1	e	0	0	0	0	1.00	0	0	0	A1	0	A1
2	578.229349	1	0	2.000000	A1	e	0	2	0	0	1.00	0	0	1	A1	0	A1
3	990.856966	1	0	2.000000	A1	e	1	0	0	0	1.00	1	0	0	A1	0	A1
4	1154.529779	1	0	4.000000	A1	e	0	4	0	0	1.00	0	0	2	A1	0	A1
5	1570.947837	1	0	4.000000	A1	e	1	2	0	0	1.00	1	0	1	A1	0	A1
6	1728.958462	1	0	6.000000	A1	e	0	6	0	0	1.00	0	0	3	A1	0	A1
7	1977.509720	1	0	4.000000	A1	e	2	0	0	0	1.00	1	1	0	A1	0	A1
8	2148.937437	1	0	6.000000	A1	e	1	4	0	0	1.00	1	0	2	A1	0	A1
9	2301.592712	1	0	8.000000	A1	e	0	8	0	0	1.00	0	0	4	A1	0	A1
10	2559.419897	1	0	6.000000	A1	e	2	2	0	0	1.00	1	1	1	A1	0	A1

Notes. i: State counting number;
$\tilde{E}$: Term value (in $\rm cm^{-1}$);
$g_{\rm tot}$: Total state degeneracy;
J: Total angular momentum quantum number;
unc: Estimated uncertainty of energy level (in $\rm cm^{-1}$);
$\Gamma_{\rm tot}$: Overall symmetry in $\boldsymbol{C}_{2v}$(M) (A_1 or A_2);
e/f: The Kronig (rotationless) parity;
v_1, $v_2^{\rm lin}$, L, v_3: Linear-molecule vibrational quantum numbers;
C_i: Largest coefficient used in the TROVE assignment;
$n_1 - n_3$: TROVE vibrational quantum numbers;
$\Gamma_{\rm vib}$: Symmetry of the vibrational contribution in $\boldsymbol{C}_{2v}$(M);
K: Rotational quantum number, projection of J on to molecule-fixed z axis ($K = L$);
$\Gamma_{\rm rot}$: Symmetry of the rotational contribution in $\boldsymbol{C}_{2v}$(M).

Table 2. Extract from the `.trans` file for the 0–100 $\rm cm^{-1}$ window of the SiO_2 OYT3 line list.

f	i	A_{if}
1901572	1832882	8.4692e-44
2283835	2261046	9.7538e-45
948596	1016760	9.4147e-35
1830303	1853859	2.7761e-42
4120223	4135284	1.1104e-41
649389	670531	1.0237e-43
284492	332334	2.6832e-31
3288298	3306461	1.3021e-31
3796784	3812806	2.0901e-39
366209	348742	3.7795e-33

Notes. f: Upper state ID; i: Lower state ID;
A_{if}: Einstein A coefficient (in $\rm s^{-1}$).

exoplanets due to the CO_2 photometric band used by the *Spitzer Space Telescope* (IRAC instrument). For example, this band was used to build the phase curve of super-Earth 55 Cancri e by Demory et al. (2016) and to provide analysis of the atmospheric (day/night) structure of the plane. The atmosphere was shown to have a high temperature contrast, from 1400 K (night side) to 2700 K (day side). In Fig. 6, we show that the CO_2 4.5 μm region has strong overlap with the spectrum of SiO_2, namely the (1, 4^0, 0) band in the same region, although the strongest absorption bands are (0, 1^1, 0) and (0, 2^2, 0) where states are labelled by the quantum numbers (v_1, v_2^L, v_3). An absorption spectrum of water is also shown for comparison. Silicon dioxide has also been suggested as a potential constituent of the atmosphere of the super-Earth Corot-7b (Schaefer et al. 2012) and thus should be included in retrievals for hot super-Earths.

4 CONCLUSION

A comprehensive molecular line list for SiO_2 has been presented. The line list, named OYT3, covers the 0–6000 $\rm cm^{-1}$ range (wavelengths $\lambda > 1.67$ μm) for states below $J = 255$ and is applicable for temperatures up to 3000 K. As discussed above, the lack of reliable experimental spectroscopic data on SiO_2 has meant that the OYT3 line list has been constructed using purely ab initio methods with no degree of empirical refinement. The accuracy of the predicted line positions will suffer as a result, particularly for highly excited states and shorter wavelengths, but for the fundamental bands, which have the strongest intensity, the errors should be within 1–3 $\rm cm^{-1}$ as a conservative estimate. The computed line intensities should not be overly affected and are largely expected to be within the 5–10 per cent of experimentally determined intensities. Of course, without reliable experimental data to compare against these are only estimates based on our previous experience constructing ab initio spectroscopic models with similar electronic structure methods (see e.g. our work on SiH_4; Owens et al. 2015b).

The usual ExoMol methodology is to take advantage of laboratory measurements to improve the accuracy of our computed line lists (Tennyson 2012). However, in the absence of high-resolution spectroscopic measurements for SiO_2, this has not proved possible. In practice a number of current line lists are entirely ab initio. Of course, for few electron systems such as HD^+ (Amaral et al. 2019), HD (Amaral et al. 2019), HeH^+ (Engel et al. 2005; Amaral et al. 2019), H_3^+ (Mizus et al. 2017), and LiH (Coppola, Lodi & Tennyson 2011) it is possible to compute high accuracy line lists which should reproduce astronomical spectra within their observational accuracy. The Molecular Opacity Database Project at the Universty of Georgia (UGAMOP) treated a number of many electron diatomics in this fashion, see Weck, Stancil & Kirby (2003) for example. However, more pertinent here is the case of HCN. The original HCN / HNC line list of Harris, Polyansky & Tennyson (2002) was based on a purely ab initio potential energy and dipole surfaces (van Mourik et al. 2001) computed at a lower level of theory, and hence of lower accuracy, than that employed here. This line list has been successively updated (Harris et al. 2006; Barber et al. 2014), and even adapted to $H^{13}CN$ (Harris et al. 2008), by the post hoc insertion of empirical energy levels, something that is explicitly allowed for

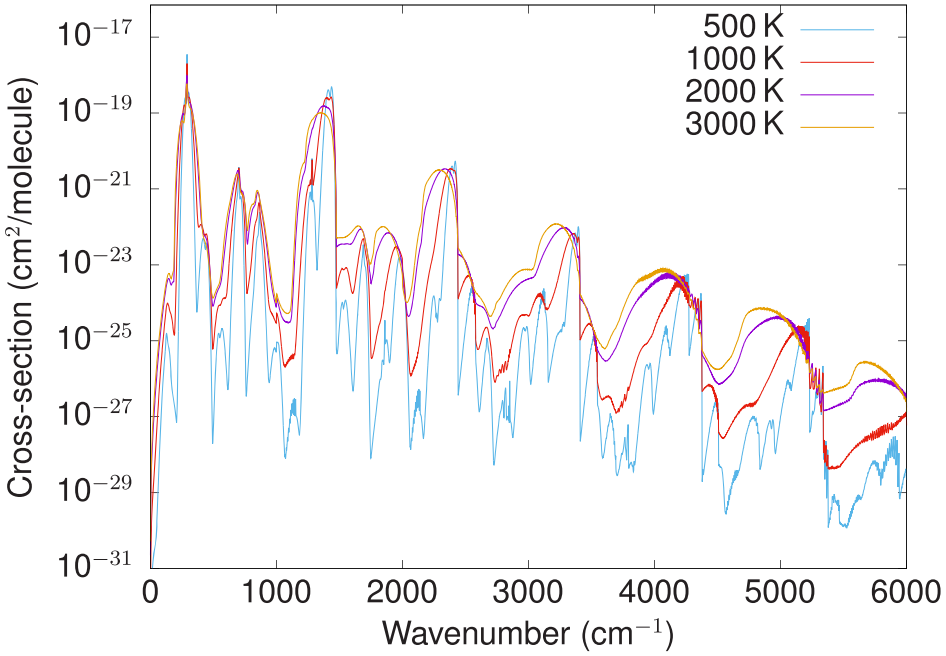

Figure 4. Temperature dependence of the spectrum of SiO_2, which becomes increasingly flat as the temperature increases. Absorption cross-sections were computed from the OYT3 line list and represented with a Gaussian line profile with a half-width at half-maximum (HWHM) of 1 cm^{-1} at a resolution of 1 cm^{-1}.

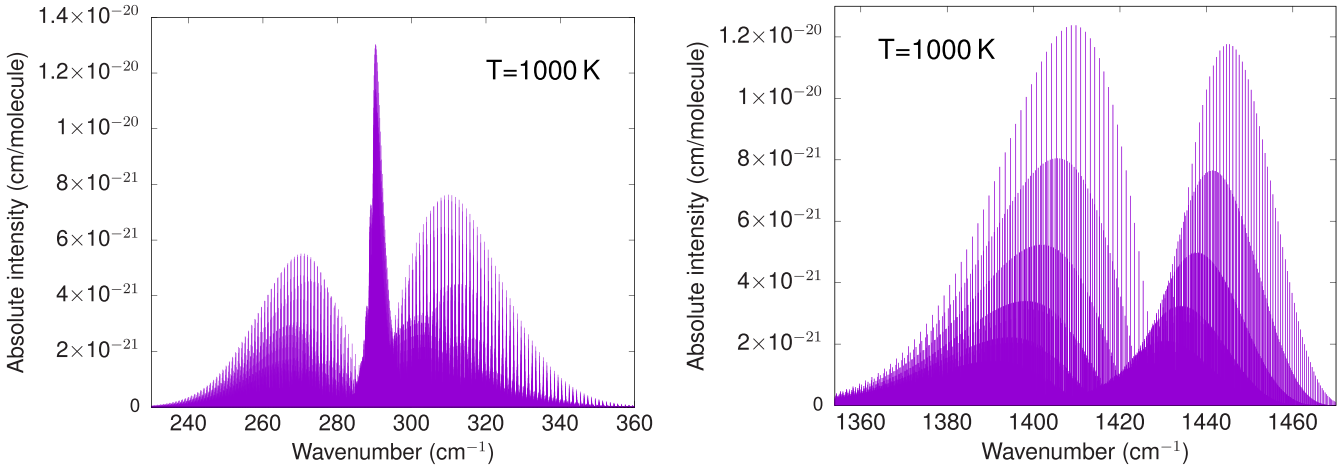

Figure 5. Stick spectrum of the two strongest bands of SiO_2 at $T = 1000$ K. The left-hand panel shows the bending ν_2 (0,1^1,0) fundamental band while the right-hand panel shows the stretching ν_3 (0,0^0,1) band, where states are labelled by the quantum numbers (v_1, $v_2{}^L$, v_3).

in the ExoMol data format (Tennyson, Hill & Yurchenko 2013). The HCN line list both in its original and updated forms has proved to be highly useful and indeed underpins a number of recent (possible) detections of HCN in exoplanets (Tsiaras et al. 2016; Hawker et al. 2018; Gandhi et al. 2020) and much exoplanet modelling; it has also been found useful for combustion studies (Glarborg & Marshall 2017). We would anticipate the OYT3 SiO_2 line list being used in a similar fashion and, should high-resolution SiO_2 spectra become available, we will update the line list to improve its accuracy. However, we are unaware of any such studies in progress at present.

For present use, we recommend the OYT3 line list for low-resolution studies of exoplanet atmospheres, e.g. with a resolving power of $R \approx 100$, but we emphasize that the line list is not designed for high-resolution analysis. Interestingly, a recent cold molecular beam study has shown that silicon dioxide can be efficiently formed through the reaction of SiH and O_2 under single collision conditions (Yang et al. 2018), demonstrating a low-temperature pathway to gas-phase SiO_2 that is plausible in the interstellar medium or molecular clouds. The OYT3 line list will aid other astronomical searches for SiO_2 and may find use in industrial processes, for example, in the semiconductor industry where silicon-bearing molecules are commonly encountered.

ACKNOWLEDGEMENTS

This work was supported by the STFC Projects No. ST/M001334/1 and ST/R000476/1. The authors acknowledge the use of the UCL Legion High Performance Computing Facility (Legion@UCL) and associated support services in the completion of this work,

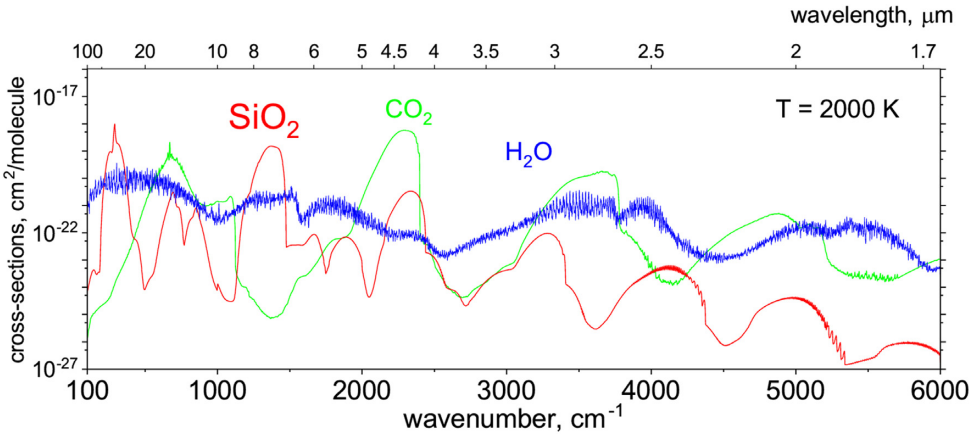

Figure 6. Comparison of the 2000 K broadband spectra of SiO_2, CO_2, and H_2O. A Gaussian line profile with HWHM of 1 cm^{-1} at a resolution of 1 cm^{-1} was used. The CO_2 cross-sections were computed using the new UCL-4000 line list (Yurchenko et al. 2020) and the Pokazatel line list for H_2O (Polyansky et al. 2018). For clarity the relatively flat water spectrum has been reduced by a factor of 10. SiO_2 shows strong absorption features around 250 and 1500 cm^{-1}. A weaker SiO_2 feature at about 2300 cm^{-1} is masked by strong CO_2 absorption in this region.

along with the Cambridge Service for Data Driven Discovery (CSD3), part of which is operated by the University of Cambridge Research Computing on behalf of the STFC DiRAC HPC Facility (www.dirac.ac.uk). The DiRAC component of CSD3 was funded by BEIS capital funding via STFC capital grants ST/P002307/1 and ST/R002452/1 and STFC operations grant ST/R00689X/1. DiRAC is part of the National e-Infrastructure.

REFERENCES

Amaral P. H. R., Diniz L. G., Jones K. A., Stanke M., Alijah A., Adamowicz L., Mohallem J. R., 2019, ApJ, 878, 95
Andrews L., McCluskey M., 1992, J. Mol. Spectrosc., 154, 223
Barber R. J., Strange J. K., Hill C., Polyansky O. L., Mellau G. C., Yurchenko S. N., Tennyson J., 2014, MNRAS, 437, 1828
Barton E. J., Yurchenko S. N., Tennyson J., 2013, MNRAS, 434, 1469
Brinkmann N. R., Tschumper G. S., Schaefer H. F., III, 1999, J. Chem. Phys., 110, 6240
Brown J. M. et al., 1975, J. Mol. Spectrosc., 55, 500
Bunker P. R., Jensen P., 1998, Molecular Symmetry and Spectroscopy, 2nd edn. NRC Research Press, Ottawa
Clark V. H. J., Owens A., Tennyson J., Yurchenko S. N., 2020, J. Quant. Spectrosc. Radiat. Transf., 246, 106929
Coppola C. M., Lodi L., Tennyson J., 2011, MNRAS, 415, 487
Demory B.-O. et al., 2016, Nature, 532, 207
Engel E. A., Doss N., Harris G. J., Tennyson J., 2005, MNRAS, 357, 471
Fegley, Jr. B., Jacobson N. S., Williams K. B., Plane J. M. C., Schaefer L., Lodders K., 2016, ApJ, 824, 103
Gandhi S. et al., 2020, MNRAS, 495, 224
Glarborg P., Marshall P., 2017, Energy Fuels, 31, 2156
Gorman M., Yurchenko S. N., Tennyson J., 2019, MNRAS, 490, 1652
Hao Y., Xie Y., Schaefer H. F., III, 2014, RSC Adv., 4, 47163
Harris G. J., Polyansky O. L., Tennyson J., 2002, ApJ, 578, 657
Harris G. J., Tennyson J., Kaminsky B. M., Pavlenko Y. V., Jones H. R. A., 2006, MNRAS, 367, 400
Harris G. J., Larner F. C., Tennyson J., Kaminsky B. M., Pavlenko Y. V., Jones H. R. A., 2008, MNRAS, 390, 143
Hawker G. A., Madhusudhan N., Cabot S. H. C., Gandhi S., 2018, ApJ, 863, L11
Jacox M. E., 1994, Chem. Phys., 189, 149
Kaufman M., Muenter J., Klemperer W., 1967, J. Chem. Phys., 47, 3365
Kostko O., Ahmed M., Metz R. B., 2009, J. Phys. Chem. A, 113, 1225
Miguel Y., Kaltenegger L., Fegley B., Schaefer L., 2011, ApJ, 742, L19
Mizus I. I., Alijah A., Zobov N. F., Kyuberis A. A., Yurchenko S. N., Tennyson J., Polyansky O. L., 2017, MNRAS, 468, 1717
Neale L., Miller S., Tennyson J., 1996, ApJ, 464, 516
Owens A., Yurchenko S. N., 2019, J. Chem. Phys., 150, 194308
Owens A., Yurchenko S. N., Yachmenev A., Tennyson J., Thiel W., 2015a, J. Chem. Phys., 142, 244306
Owens A., Yurchenko S. N., Yachmenev A., Thiel W., 2015b, J. Chem. Phys., 143, 244317
Owens A., Yurchenko S. N., Yachmenev A., Tennyson J., Thiel W., 2016, J. Chem. Phys., 145, 104305
Owens A., Yurchenko S. N., Yachmenev A., Thiel W., Tennyson J., 2017, MNRAS, 471, 5025
Owens A., Yachmenev A., Küpper J., Yurchenko S. N., Thiel W., 2018, Phys. Chem. Chem. Phys., 21, 3496
Pacansky J., Hermann K., 1978, J. Chem. Phys., 69, 963
Polyansky O. L., Kyuberis A. A., Zobov N. F., Tennyson J., Yurchenko S. N., Lodi L., 2018, MNRAS, 480, 2597
Schaefer L., Fegley B., 2009, ApJ, 703, L113
Schaefer L., Lodders K., Fegley B., Jr, 2012, ApJ, 755, 41
Schnöckel H., 1978, Angew. Chem. Int. Ed. Engl., 17, 616
Schnöckel H., 1980, Z. Anorg. Allg. Chem., 460, 37
Tennyson J., 2012, WIREs Comput. Mol. Sci., 2, 698
Tennyson J., 2014, J. Mol. Spectrosc., 298, 1
Tennyson J., 2016, J. Chem. Phys., 145, 120901
Tennyson J., Yurchenko S. N., 2012, MNRAS, 425, 21
Tennyson J., Yurchenko S. N., 2017a, Mol. Astrophys., 8, 1
Tennyson J., Yurchenko S. N., 2017b, Int. J. Quantum Chem., 117, 92
Tennyson J., Yurchenko S. N., 2018, Atoms, 6, 26
Tennyson J., Kostin M. A., Barletta P., Harris G. J., Polyansky O. L., Ramanlal J., Zobov N. F., 2004, Comput. Phys. Commun., 163, 85
Tennyson J., Hill C., Yurchenko S. N., 2013, in AIP Conf. Proc. Vol. 1545, 6th international conference on atomic and molecular data and their applications ICAMDATA-2012. AIP, New York, p. 186
Tennyson J. et al., 2016, J. Mol. Spectrosc., 327, 73
Tsiaras A. et al., 2016, ApJ, 820, 99
Upadhyay A., Conway E. K., Tennyson J., Yurchenko S. N., 2018, MNRAS, 477, 1520
van Mourik T., Harris G. J., Polyansky O. L., Tennyson J., Császár A. G., Knowles P. J., 2001, J. Chem. Phys., 115, 3706

Wang L.-S., Wu H., Desai S. R., Fan J., Colson S. D., 1996, J. Phys. Chem., 100, 8697
Weck P. F., Stancil P. C., Kirby K., 2003, J. Chem. Phys., 118, 9997
Yang T., Thomas A. M., Dangi B. B., Kaiser R. I., Mebel A. M., Millar T. J., 2018, Nat. Commun., 9, 774
Yurchenko S. N., 2014, in Springborg M., Joswig J.-O., eds, Chemical Modelling: Vol. 10, The Royal Society of Chemistry, Cambridge, p. 183
Yurchenko S. N., Thiel W., Jensen P., 2007, J. Mol. Spectrosc., 245, 126
Yurchenko S. N., Yachmenev A., Ovsyannikov R. I., 2017, J. Chem. Theory Comput., 13, 4368
Yurchenko S. N., Al-Refaie A. F., Tennyson J., 2018, A&A, 614, A131
Yurchenko S. N., Tennyson J., Miller S., Melnikov V. V., O'Donoghue J., Moore L., 2020, MNRAS, in press

SUPPORTING INFORMATION

Supplementary data are available at *MNRAS* online.

SiO2_SI_2402.pdf

Please note: Oxford University Press is not responsible for the content or functionality of any supporting materials supplied by the authors. Any queries (other than missing material) should be directed to the corresponding author for the article.

This paper has been typeset from a TEX/LATEX file prepared by the author.